# AIAA Paper
# No. 69-402



## EXPERIMENTAL STUDY OF THE EFFECTS OF SWEEP ON HYDROFOIL LOADING AND CAVITATION

by

PETER CRIMI
Rochester Applied Science Associates, Inc.
Rochester, New York

**AIAA**
**2nd Advanced Marine Vehicles and Propulsion Meeting**
SEATTLE, WASHINGTON / MAY 21-23, 1969

# EXPERIMENTAL STUDY OF THE EFFECT8 OF SWEEP ON HYDROFOIL LOADING AND CAVITATION'

Peter Crimi**
Rochsmter Applied Science Associates, Inc.
Rochester, New York

## Abstract

An experimental program was conducted to investigate the relationship of sweep angle to cavitation inception on hydrofoils and to deterioration of hydrofoil performance due to cavitation. Teats were carried out in a water tunnel on a series of four conmtant-chord ● emimpan hydrofoil models with mweep anglem of 0, 15, 30 and 4 5 degrees, rempectively. Measurement8 of lift and drag were made, varying incidence and cavitation number for each model.

The results obtained show a considerable increase in the mpeed for cavitation inception with increasing sweep angle. Alma, the ● peed for effectively subcavitated operation, am meamured by performance, was found to increase significantly with increaming mweep angle. The latter gain8 were in evidence from a determination of the variation with forward ● pined of maximum lift-drag ratio and of drag at constant lift.

## Nomenclature

| | |
|---|---|
| A | foil area, $ft^2$ |
| $C_D$ | drag coefficient - $C_D = D/(1/2\rho V^2 A)$ |
| $C_L$ | lift coefficient - $C_L = L/(1/2\rho V^2 A)$ |
| $C_{L_1}$ | lift coefficient at $\sigma$ = 1 when lift is held conmtant |
| D | drag, lb |
| L | lift, lb |
| $p_c$ | vapor premmure of water, paf |
| $p_\infty$ | free-•tream static pressure, psf |
| V | free-•tremm speed, ft/sec |
| θ | foil angle of attack, deg |
| Λ | sweep angle, deg |
| ρ | free-•tremm mass density, ● lugm/LtS |
| σ | cavitation number - , |

$$\sigma = (p_\infty - p_c)/(1/2\rho V^2)$$

## Introduction

A major factor in the design of hydrofoil boats is the limitation in performance imposed by cavitation. The presence of a cavity of vapor, canaed by the lowering in pressure on the suction aide of the foil down to the vapor pressure of the water, causes a very large reduction in lift and a large increase in drag. In addition, the lifting surfaces can be seriously eroded by cavitation when operated at or near cavitation inception. Thus, the designer is faced with 'the choice of either limiting the speed of the craft to avoid cavitation or accepting large losses in efficiency and penalties in power required.

It can be shown through a straightforward analymim that the maximum speed for mubcavitatfng flight can be increased submtantially by utilizing sweepback. This effect derivem from the same principle as the one manifemted in forestalling of compressibility effects on swept aircraft wings. That is, the loading on a given wing section is nearly independent of the apanwise component of the flow so the speed for cavitation inception is only determined by the flow component normal to the leading edge. If the foil is swept, the forward mpeed of the craft at which cavitation occurs mumt then increase. This effect can be put on a quantitative basis by analyzing an infinite yawed foil, as outlined in the Appendix. The ● tudy reported here was directed to determining experimentally whether, for a hydrofoil of finite span, the mpeed at which cavitation occurs can be increamed ● ignificantly, to give corresponding gains in performance, by employing mweep.

Sweeping of the foil undoubtedly ham detrimental ● ffectm on some aspects of performance . There is a loss in lift effectivenems with increasing ● weep angle. The boundary layer may build up near the tips, mm it does on swept aircraft wings, giving rise to unfavorabio stall characteristics and attendant difficulties in taking off. ventilation of mtrutm (struts ● hould also be swept, of course) may be difficult to prevent at the higher speeds. Also, the distribution of loading may ● dvermely ● ffeat stability and control. Some of the disadvantages may be countered, however, by employing variable ● wuap, which is more ● amily implemented on a hydrofoil craft than on an aircraft.

The specific objective of thim study was to determine whether a foil of finite aspect ratio, with spanwise loading variations, cavitates et a speed determine4 primarily from tha chordwise flow component. Tests were aonduoted in the 12-inch water tunnel at ths Ordnance Research Laboratory, Pennsylvania State University, on a series of four oonmtmnt-chord, semispan hydrofoil

*This research was carried out under the Naval Ship Systems Command General Hydromechanics Research Program, Subproject SR 009 01 01, ● 4mIinimterod by tha Naval ship Research and Development Center.

**Senior Research Engineer.

models. The models had sweep angles of 0, 15, 30, and 45 degrees. Measurements were taken of the lift and drag as a function of incidence and cavitation number. The test facility, models, and mounting and measuring apparatus are described next. The results of the tests are then discussed.

## Test Facility, Models and Test Apparatus

### Test Facility

The tests were conducted in the closed-circuit water tunnel having a 12-inch circular test section at the Ordnance Research Laboratory, Pennsylvania State University. The tunnel provides a wide range of cavitation numbers. Flows of up to 80 feet per second with test-section static presaures from 3 to 60 psia can be obtained.

The upper leg of the water tunnel, including the test section with the mounting apparatus of the subject tests installed, is shown in Figure 1. Further details of the facility are available in a report describing the tunnel and its capabilities.(1)

### Hydrofoil Models

A series of four constant-chord, semi-span hydrofoil models were tested, with sweep angles of 0, 15, 30, and 45 degrees, respectively. All models had the same area and the same chord and foil section taken normal to the leading edge.

The model planforms are as indicated in Figure 2. The basic zero-sweep model has a span of 6 inches and a chord of 2 inches, giving an aspect ratio of six for full-span flow, as approxfmated through the use of a splitter plate. The span was chosen to avoid wall interference in the 12-inch test section of the water tunnel. The chord was selected to give as high an aspect ratio as possible without imposing severe structural requirements. The tang for each model is the same, and is designed to fit a common clamping device attached to the measuring apparatus.

The foil section normal to the leading edge has the NACA designation of 16-309. A sketch of the 16-309 section and a listing of offsets is given in Figure 3. This section has a maximum thickness of nine percent of chord. The maximum thickness is located six tenths of the chord from the leading edge. The 16-309 section is well suited to subcavitating operation because it has a relatively low suction peak at its design lift coefficient of 0.30. It has been utilized previously in at least two experimental programs (2,3) and on the U. S. Navy's PC (H) "High-point" hydrofoil craft.

Each model, with integral tang, was cut from a single workpiece of heat-treated 416 stainless steel. The use of exceptionally strong material and, the avoidance of welded construction were dictated by the high bending stresses anticipated at the root at low cavitation numbers.

### Mounting and Measuring Apparatus

The mounting and measuring apparatus which was fabricated is shown schematically in Figure 4. Photographs of the various components of the apparatus are shown in Figure 5a and the complete assembly is shown in Figure 5b.

As can be seen from the figures, the apparatus consists basically of a water-filled cylinder mounted on a plate which mates with an opening in the circular test section of the water tunnel. Fastened to the end plate of the cylinder are two elements for measuring forces normal and tangent to the foil chord, respectively. These elements take up the force component to be measured through tension members. The unit has high natural *frequency* and gives force readings which are minimally affected by applied torque. The clamp which holds the models bolts to a flange on the outer force-measuring element. The model projects through a slot in a circular insert in a rectangular splitter plate. The splitter plate is screwed to the tunnel wall. Foil incidence is changed by loosening six bolts and rotating the cylinder through the desired angle, as indicated by a scale attached to the unit (see Figure 5b).

## Discussion of Results

### Basic Data - Characterization of Flows

The tests were generally conducted on each model in the following manner. First, foil incidence was selected and the tunnel was brought up to speed. The free-stream speed was made as high as possible, without giving excessive loads, in order to maintain a high Reynolds number and to provide good force readings. Once tunnel speed was stabilized, test-section static pressure was lowered in steps from a value somewhat above atmospheric pressure. Force readings, tunnel static and dynamic pressures and water temperature were recorded after each change in static pressure. The character and extent of cavitation, if any, was observed and recorded.

When sufficient data was obtained at a given incidence, tunnel pressure was returned to above atmospheric, tunnel speed was lowered, foil incidence was changed and the test procedure repeated. Runs were made for angles of attack from -4 degrees to 10 degrees in 2-degree increments.

The basic data was derived from these runs, with the variation of lift coefficient $C_L$ and drag coefficient $C_D$ determined as a function of cavitation number $\sigma$ for a given angle of attack $\alpha$ and sweep angle $\Lambda$. The force coefficients and cavitation number are defined by

$$C_L = \frac{L}{1/2\rho V^2 A}$$

$$C_D = \frac{D}{1/2\rho V^2 A}$$

$$\sigma = \frac{p_\infty - p_c}{1/2\rho V^2}$$

where L and D are components of hydrodynamic force normal and parallel, respectively, to the free stream: V is free-stream speed: $\rho$ is water density; A is foil area (12 square inches for all models); $p_\infty$ is free-stream static pressure and pc is the vapor pressure of the water. The maximum errors incurred through recording and reducing the data are estimated to be, in general, from 1% to 2% in $C_L$, from 2% to 4% in $C_D$, and from 1% to 2% in σ. A complete tabulation of the data obtained is given in Reference 4.

A representative variation of the force coefficients with cavitation number is illustrated by the curves of Figurer 6, 7, and 8. In those figures, CL, $C_D$, and L/D, respectively, are plotted aqainmt σ for α = 8°, for both Λ = 0° and Λ = 45°. The identifying labels appearing with certain of the points are the figure numberm of photographs taken of the model when the data for those points were recorded. Thus, the photographs of the zero-sweep model are shown in Figures 9a through 9d and thome of the model with 45-degree sweep are given in Figures 10a through 10d.

Following the curves from the araa of fully wetted Slow in the direction of decreasing σ, the Sirot noticeable change is a rise in the $C_L$-curves (Figure 6), beqinning at about σ = 2.6 for Λ = 0° and at about σ = 1.9 for Λ = 45°. It was found through analyria of photographs and notes made while data was being taken that the paint at which $C_L$ begins to increase generslly marks the inception of cavitation. At about the same value of σ, or slightly less, the $C_D$-curves also begin to rise.

Upon continuing into the region of partially cavitated flow, A maximum in the $C_L$-curve is noted, at σ = 1.1 for Λ = 0° And At σ = 0.67 for Λ = 45°. The maximum in CL was Sound to occur, generally, when tho foil WAS about 50% cavitated, for Λ = 0°. There was some increase in the extent of cavitation at the point of maximum $C_L$ with increasing Λ, there generally being from 70 to 75% of the foil ● ree cavitated with Λ = 45°.

Next, there are maximums in the $C_D$-curves (Figure 6) which occur At a still lower cavitation number. The peak for Λ = 0° is at σ = .8 and, for Λ = 45°, it is at σ = .6. The maximum in $C_D$ appears to correspond, for all sweep angles, to the cavitation number at which the foil is just fully cavitated.

Note that the curves of L/D versus σ (Figure 7) do not have maxima or minima, but instead decrease monotonically with decreasing σ. Apparently the maximum in $C_L$ is just sufficiently separated from the peak in $C_D$ to make their ratio vary monotonically.

A good qualitative indication of the effects of sweep on cavitation can be obtained from a comparison of the photographs in Figurer 9 and 10. Note, first, that both the tip and root sections remain wetted when the unswept foil is partially cavitated. The swept foil, on the other hand, can be seen to experience cavitation over the tip, And A good deal more of the root section is wetted, under comparable conditions.

Rather more by good fortune than intent, the photographs of Figures 8 and 9 were taken, for each model, At nearly the mane cavitation numbers. That is, the flows pictured by Figures 8a and 9a are at nearly the same cavitation number, 8b and 9b correspond to about the same value of σ, etc. Although the lift coefficients for Λ = 45° are considerably smaller than thoae for Λ = 0°, due to the loos in lift effectiveness, the aaaea for the two sweep anqlem are still comparable, mince the L/D-curvem are not nearly so widely ● eparAted. The difference in the L/D-curves is probably due to the lower aspect ratio of the ● wept model. Note that the extent of cavitation of the swept model is considerably less than on the unswept one, at All four cavitation numberm. The effect is evident [illegible] ● atimatem which were made of the Areas cavitated in the photographs and are listed below.

| Λ-deg. | Figure No. | Cavitation No. σ | Estimated Percent Area Cavitated |
|---|---|---|---|
| 0 | 9a | 1.794 | 14.9 |
| | 9b | 1.093 | 55.6 |
| | 9c | 0.837 | 96.0 |
| | 9d | 0.612 | ~100.0 |
| 45 | 10a | 1.681 | 3.3 |
| | 10b | 1.046 | 31.9 |
| | 10c | 0.771 | 45.3 |
| | 10d | 0.594 | 85.0 |

## Effect of Sweep on Cavitation Inception

The relationship between foil sweep Angle and the speed at which cavitation first occurs to any noticeable degree is of particular interest in relation to the problem of cavitation damage. The determination of the cavitation number at which cavitation first appears was found difficult to make with any precision by observing the flow. However, as was noted previously, inception seems generally to occur at the cavitation number at which the lift coefficient begins to increase..

For the purposes of this report, then, inception is defined as that point on the CL versus σ curve at which CL begins to rise. In order to determine the variation of cavitation number for inception, working plots of the lift coefficient as a function of σ for each angle of attack and sweep angle, similar to those of Figure 6, were first constructed. The point of inception was then determined according to the above definition. A plot was then constructed of the cavitation number at inception as a function of lift coefficient, for each of the four sweep angles. Those curves are shown In Figure 11.

As can be seen from Figure 11, the effect of sweep on cavitation is clearly noticeable. For $\Lambda = 45°$, the minimum value for σ at inception is 0.22, and for $\Lambda = 0°$, that minimum point is 0.35, giving a ratio of free-stream speeds of 1.26. That the benefit of sweep is not as noticeable as might be expected for $\Lambda = 15°$ and $\Lambda = 30°$ must be due to effects of finite aspect ratio. The value of σ at inception is proportional to $\cos^2\Lambda$ in the two-dimensional came (See the Appendix), which variation would give considerably more spread to the curves in the region of the minima, for the three lowest sweep angles.

## Effect of Sweep on Performance

Two aspects of the relationship of cavitation to the performance of swept foils were investigated. Specifically, the data was analyzod to extract operating efficiency, as measured by the maximum lift-drag ratio as a function of cavitation number, and by the power required for a specific design, as reflected by the variation of drag with forward speed for constant lift.

The variation of the maximum in L/D with cavitation number was determined in the following way. First, working plots of L/D versus σ were constructed for each value of α and Λ. Then, cross plots were generated of L/D versus α with σ as a parameter, for each sweep angle. The maximum was then read off each cross plot, to form the curves shown in Figure 12. The abscissa of those plots is $\sigma^{-1/2}$, which is proportional to forward speed when water temperature and static pressure are held fixed.

From Figure 12, it can be seen that sweeping of the foil increases the speed at which cavitation causes a deterioration in performance. The maximum L/D begins to drop off rapidly at about $\sigma^{-1/2} = 1.3$ for $\Lambda = 0°$, while, for $\Lambda = 45°$, the drop-off point is at $\sigma^{-1/2} = 2.0$. The decrease in maximum L/D with sweep angle for the fully wetted foils is due primarily to the decrease in aspect ratio with increasing sweep angle (the zero-sweep model has a-full-span-aspect ratio of six, while that of the model with $\Lambda = 45°$ is three) and so is recoverable. No explanation can be offered for the somewhat anomalous behavior of the model with 15 degrees of sweep, other than to note that the larger L/D is due to a decrease in drag, rather than an increase in lift, as Λ is changed from 0 degrees to 15 degrees.

The variation of drag with forward speed for constant lift (i.e., for a given ship) was derived as follows. From working plots of $C_L$ and $C_D$ versus σ, cross-plots of the lift and drag coefficients as a function of angle of attack α, with σ as the parameter, were generated. It was then hypothesized that the lift, L, is a constant. But the lift coefficient, CL', must still vary with forward speed V, as must the cavitation number. It is readily shown that CL must be proportional to σ if L is constant:

$$C_L = C_{L_1}\sigma$$

where $C_{L_1}$ is the value of $C_L$ at $\sigma = 1$. Thus, some value, say 0.4, would first be selected for $C_{L_1}$. Then, the value of $C_L$ at appropriate values of σ would be calculated from the above relation. The cross-plot of $C_L$ versus σ was then consulted to determine the value of α for each $C_L$ value which was calculated. Given α, the drag coefficient could be taken off the plot of $C_D$ versus σ and the ratio $C_D/C_L = D/L$ computed. The ratio D/L is plotted against $\sigma^{-1/2}$ in Figures 13, 14 and 15, for values of CL, of 0.2, 0.4 and 0.6, respectively.

The plots of Figures 13 through 15 can be regarded as showing the variation, in non-dimensional terms, of drag with forward speed. The plots can be seen to show a clear performance advantage for swept foils. The sharp rise in drag as speed is increased can be attributed to cavitation. The points of cavitation inception, obtained from Figure 11, which are indicated by a small arrow on each curve, are seen to occur at a speed in the vicinity of the sharp drag rise in Figures 13 and 14. In Figure 15, with $C_{L_1} = 0.6$, the high loading causes

*Some cavitation generally occurred at the intersection of the root with the splitter plate at somewhat higher cavitation numbers. However, premature cavitation in this region could presumably be eliminated by more careful design.

cavitation to occur at all speeds except for a small region near the minimum for $\Lambda = 0°$. It can still be inferred, however, that the drag rise is due to cavitation in this came as well.

The shift to higher speed with increasing sweep angle of the drag rise due to cavitation can be seen for all three values of $C_{L_1}$. The largest gain appears to be for $C_{L_1} = 0.4$ (Figure 14), where the curve for $\Lambda = 45°$ is shifted by an increment of about 0.43 in $\sigma^{-1/2}$ with respect to the curve for $\Lambda = 0°$. This increment represents an increase in speed of about 12.0 knots for $p_\infty - p_c = 15$ psi.

## Conclusions

The results obtained indicate that there are clear advantages to be obtained from sweeping a hydrofoil. The speed at which cavitation inception occurs is increased with increasing sweep angle, so sweep should alleviate the problem of erosion due to cavitation. The speed for effectively subcavitated operation, as measured by performance, is increased by sweeping the foil, as was seen from plots against forward speed of maximum lift-drag ratio and of drag at constant lift with sweep angle as parameter.

The effects of aspect ratio were clearly evident in the data. This would indicate that the influence of foil planform and other parameters, such as built-in twist and proximity to a free surface, should be taken into account if sweep is being considered for a specific application.

## Appendix

### Two-dimensional Analysis of the Effect of Sweep on Cavitation Inception

Consider an infinite yawed cylinder in an incompressible, inviscid flow of magnitude V, as represented in Figure 16. The flow must be independent of $\eta$ and is assumed to be irrotational, so the flow component in the $\eta$-direction must be constant and of magnitude V sin $\Lambda$. Further, let $f(\xi,\eta)$ denote the magnitude of the gradient of the velocity potential of the two-dimensional flow about a section of the cylinder taken normal to the $\eta$-axis, for a free stream of unit magnitude. Then the magnitude of the component in the $\xi$-$\zeta$ plane is $fV \cos\Lambda$. From Bernoulli's equation, the static pressure p at any point is then given by:

$$p = p_\infty - \frac{1}{2}\rho V^2 (f^2 - 1)\cos^2\Lambda \qquad (1)$$

where $p_\infty$ is the free-stream static pressure and $\rho$ is the fluid density. Thus, if $p_c$ is the vapor pressure and $\lambda$ is the maximum value of $f$, the inception of cavitation occurs at a speed $V_c$, where, from Eq. (1),

$$V_c = \frac{1}{\cos\Lambda}\left[\frac{2(p_\infty - p_c)}{\rho(\lambda^2 - 1)}\right]^{1/2} \qquad (2)$$

Thus, the speed for cavitation inception on an infinite yawed foil varies inversely as the *cosine* of the sweep angle. If, for example, $\lambda = 1.188$, which is representative of subcavitating sections, then increasing $\Lambda$ from zero to 45 degrees increases Vc from about 43 knots to 60 knots.

## References


1. Lehman, A.F., "The Glarfield Thomas Water Tunnel," Penn. State Univ., Univ. Park, Pa., Ordnance Research Lab. Rept. No. NOrd 16597-56, September 1959.

2. Feldman, J., "Experimental Investigation of Near-surface Hydrodynamic Force Coefficient8 for a Systematic Series of Tee Hydrofoils, DTMB Series HF-1," David Taylor Model Basin, Hydromechanics Lab. Research and Development Rpt. No. 1801, December 1961.

3. Conolly, A.C., "Results of Some Recent Hydrofoil Work," J. Aircraft, Vol. 2, No. 5, September-October 1965.

4. Crimi, P., "Experimental Study of the Effects of Sweep-on Hydrofoil Loading and Cavitation," Rochester Applied Science Associates Rept. No. 68-14, December 1968.


**Figure** 1. **Water** tunnel upper leg with model mounting apparatus installed in the test section.

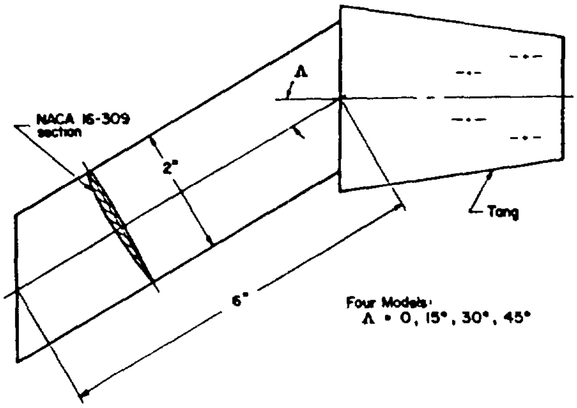


Figure 2. Model planforms.

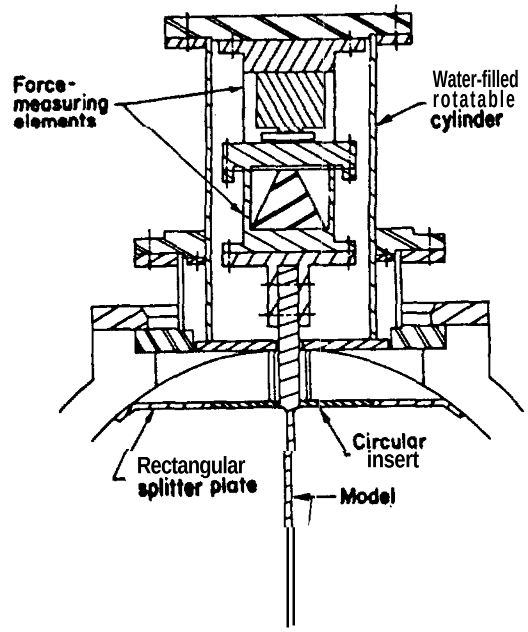


Figure 4. Schematic of mounting and measuring apparatus.

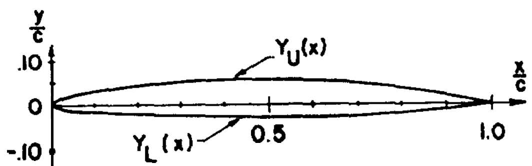


| $100\frac{x}{c}$ | $00\frac{Y_U}{c}$ | $100\frac{x}{c}$ | $100\frac{Y_L}{c}$ |
|---|---|---|---|
| 0.0 | 0.0 | 0.0 | 0.0 |
| 1.149 | 1.125 | 1.351 | 0.803 |
| 2.382 | 1.628 | 2.618 | 1.070 |
| 4.668 | 2.351 | 5.132 | 1.403 |
| 7.364 | 2.906 | 7.636 | 1.634 |
| 9.864 | 3.365 | 10.14 | 1.813 |
| 14.87 | 4.108 | 15.13 | 2.088 |
| 19.88 | 4.690 | 20.12 | 2.302 |
| 29.92 | 5.520 | 30.08 | 2.604 |
| 39.96 | 5.998 | 40.04 | 2.784 |
| 50.00 | 6.155 | 50.00 | 2.845 |
| 60.04 | 5.983 | 59.95 | 2.769 |
| tone | 5.409 | 69.92 | 2.493 |
| 80.10 | 4.341 | 79.90 | 1.953 |
| 90.10 | 2.661 | 89.90 | 1.109 |
| 95.08 | 1 532 | 94.93 | .584 |
| 100.00 | .09C | 100.00 | .090 |

Figure 3. The NACA 16-309 foil section and listing of offsets

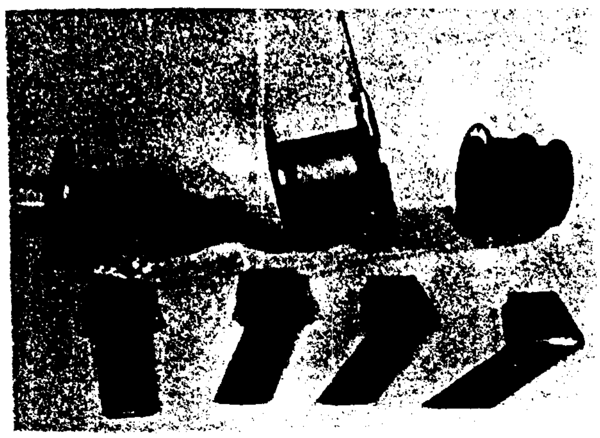

5a

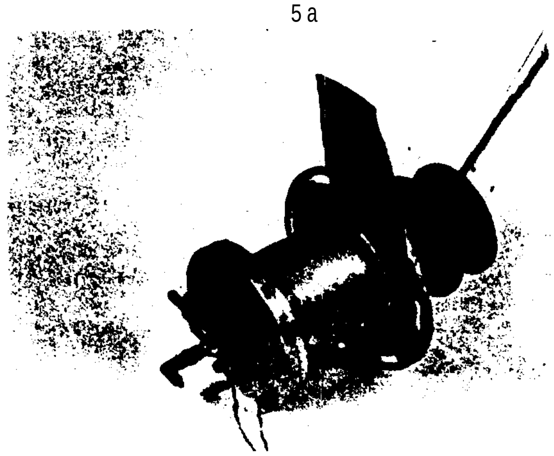

5b

Figure 5. Test apparatus components and assembly.

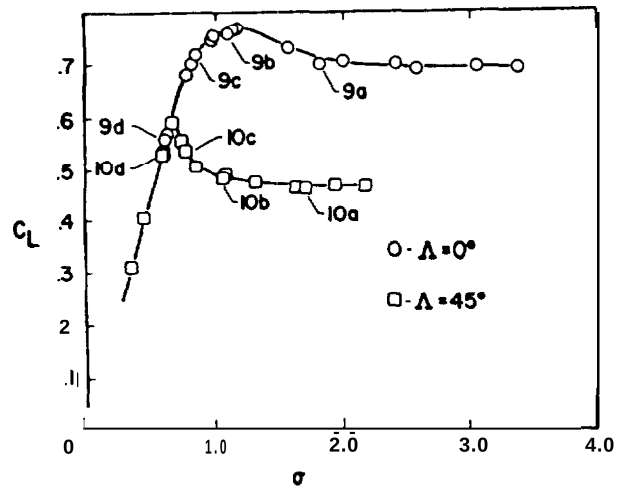


Figure 6. Variation of $C_L$ with σ at α = 8° for Λ = 0° and Λ = 45°.

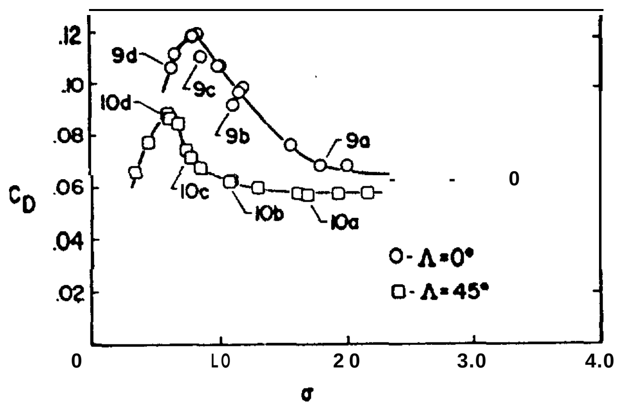


Figure 7. Variation of $C_D$ with σ at α = 8° for Λ = 0° and Λ = 45°.

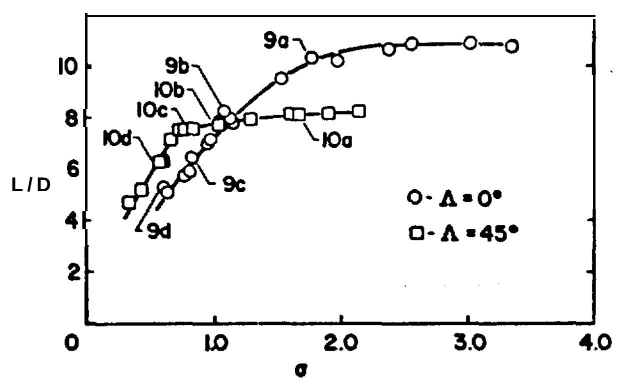


Figure 8. Variation of L/D with σ at α = 8° for Λ = 0° and Λ = 45°.

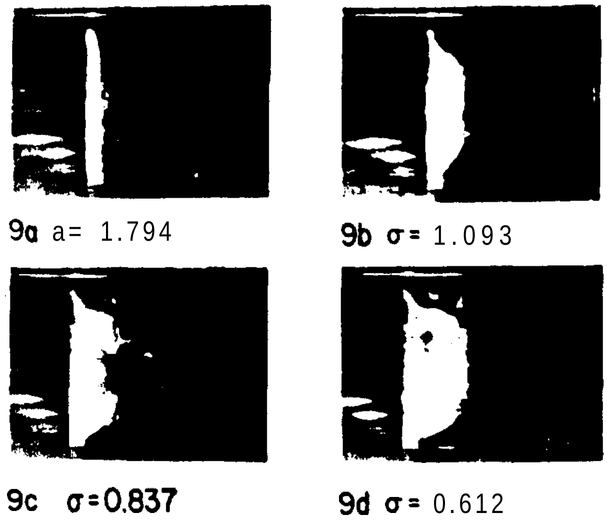


Figure 9. Extent of cavitation at four different cavitation numbers for α = 8°, Λ = 0° (see Figures 6, 7 and 8)

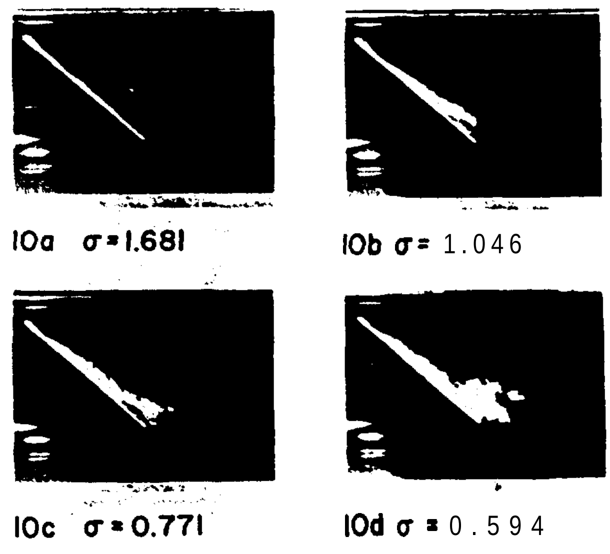


Figure 10. Extent of cavitation at four different cavitation numbers for α = 8°, Λ = 45° (see Figures 6, 7 and 8).

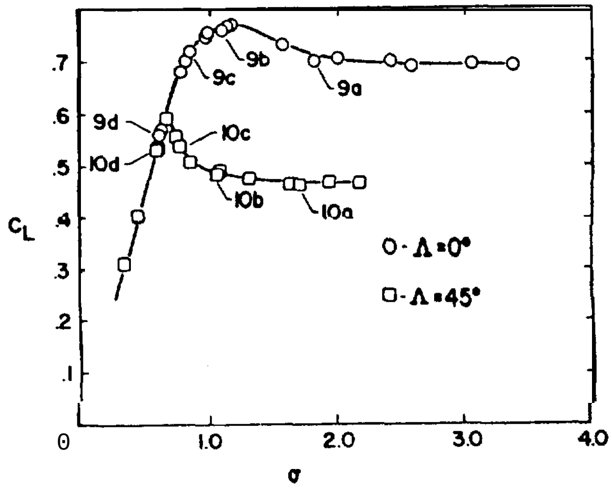


Figure 6. Variation of $C_L$ with σ at α = 8° for Λ = 0° and Λ = 45°.

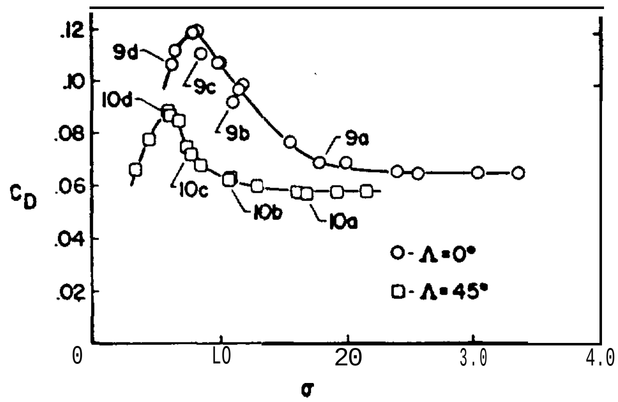


Figure 7. Variation of $C_D$ with σ at α = 8° for Λ = 0° and Λ = 45°.

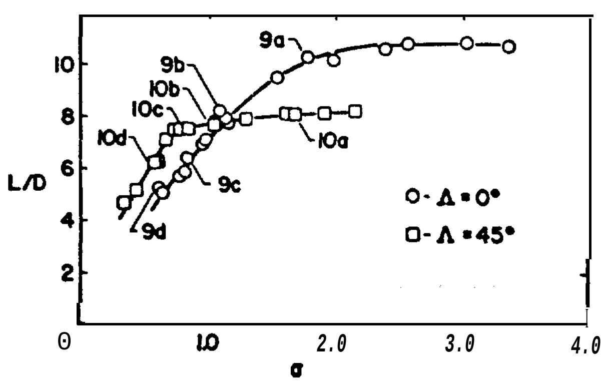


Figure 8. Variation of L/D with σ at α = 8° for Λ = 0° and Λ = 45°.

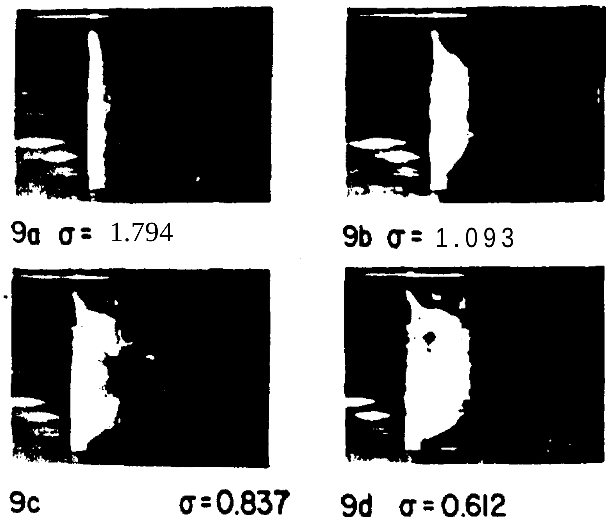


Figure 9. Extent of cavitation at four different cavitation numbers for α = 8°, Λ = 0° (see Figures 6, 7 and 8)

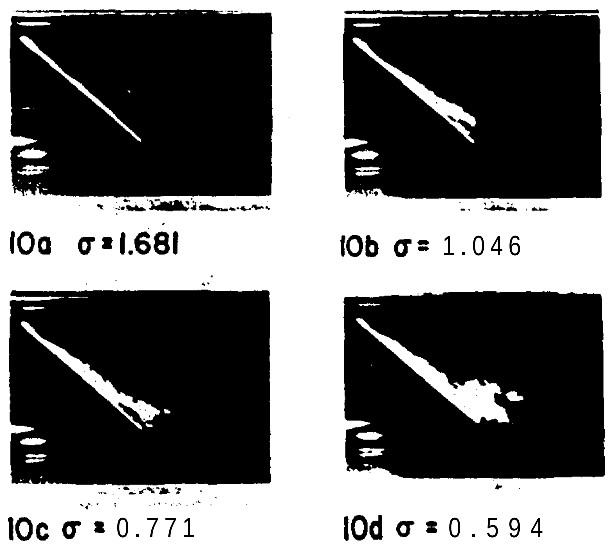


Figure 10. Extent of cavitation at four different cavitation numbers for α = 8°, Λ = 45° (see Figures 6, 7 and 8).

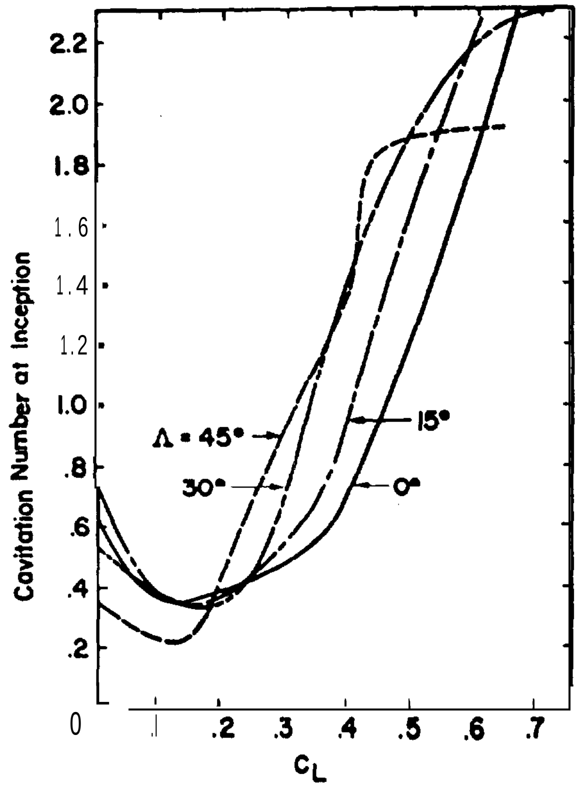


Figure 11. Cavitation number at inception as a function of lift coefficient.

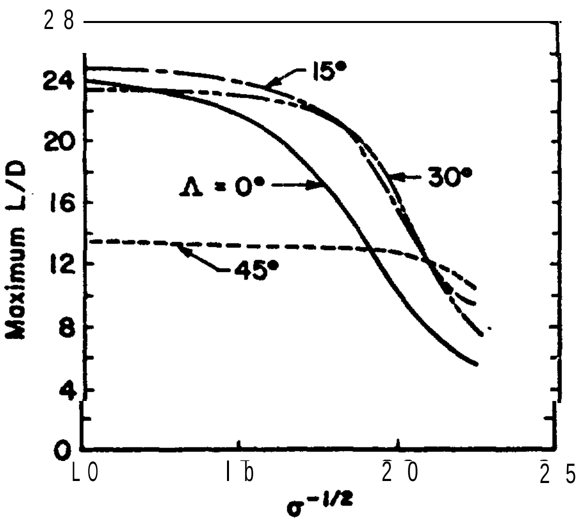


Figure 12. Maximum L/D vs. $\sigma^{-1/2}$

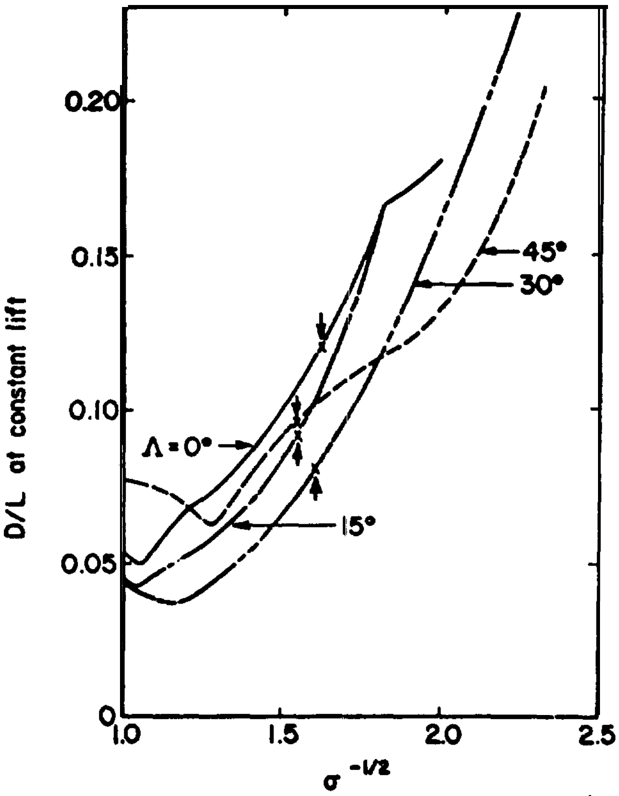


Figure 13. D/L at constant lift vs. $\sigma^{-1/2}$ for $C_{L_1}$ = 0.2.

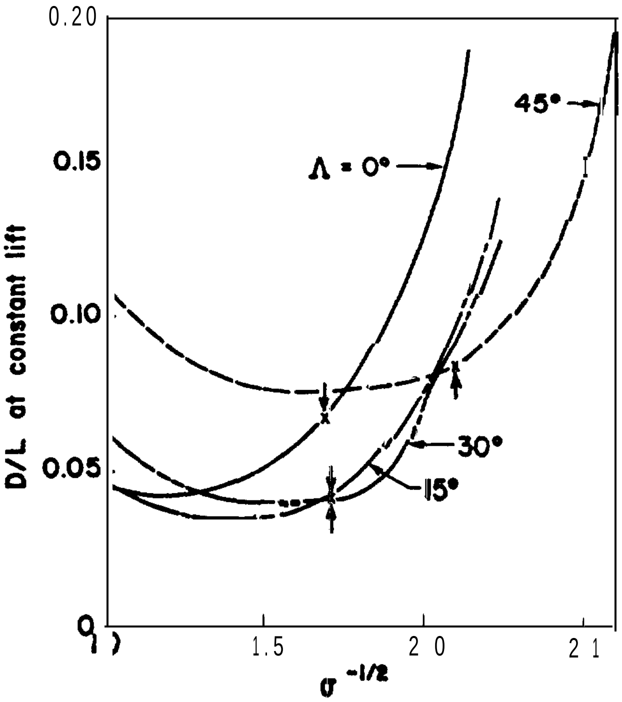


*Figure 14.* D/L at constant lift vs. $\sigma^{-1/2}$ fox $C_{L_1}$ = 0.4.

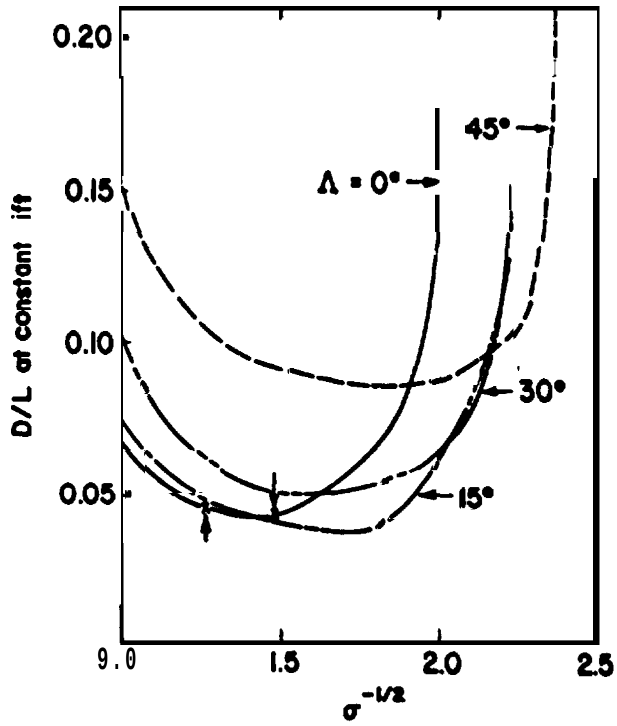


**Figure** 15. D/L at constant lift **vs.** $\sigma^{-1/2}$ for $c_{L_1}$ = 0.6.

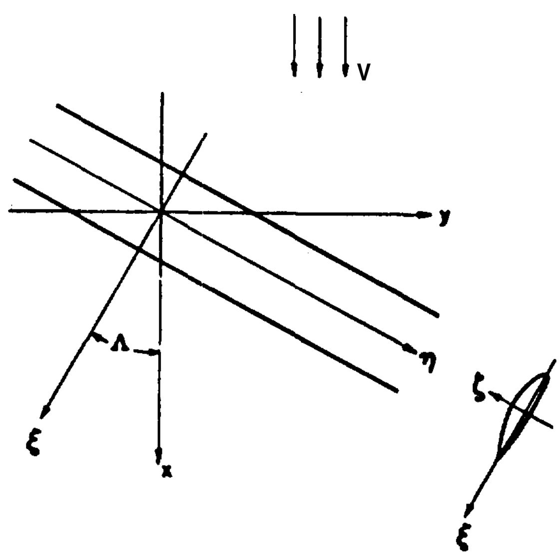


**Figure** 16. Coordinates **for** an infinite **yawed cylinder.**